https://doi.org/10.59761/RCR5231

Engineering of specific composite silica nanoarchitectures with d-transition metal ions, complexes, oxides and sulfides for MRI contrast agents and nanocatalysts

Olga D. Bochkova, Alexey S. Stepanov, Anastasiya P. Bebyakina, Asiya R. Mustafina

A.E.Arbuzov Institute of Organic and Physical Chemistry, Kazan Scientific Center, Russian Academy of Sciences, 420088 Kazan, Russian Federation

The practical significance of silica nanoparticles (SNPs) loaded with metal ions/complexes and/or metal oxides/sulfides stimulates the search for optimal one-pot synthesis methods that allow controlling both the size, shape, polydispersity of composite nanoparticles and changes occurring with metal compounds during the synthesis. To achieve this goal, it is necessary to understand the fundamental aspects of the synthetic loading of SNPs with metal compounds. These aspects include the influence of coordination and oxidative transformations of metal compounds, as well as their interaction with silica seeds, on the colloidal and functional properties of composite SNPs. The influence of the ligand, metal ion, or synthesis method, with or without surfactants, is considered as a tool for controlling the properties of composite SNPs. A comparative analysis of the use of the Stöber and water-in-oil microemulsion methods for growing SNPs containing iron/copper oxides/sulfides, 3(4)d metal ions, and their complexes as practically significant additives is also presented. Both the influence of accompanying additives and the variation of the time conditions of their stepwise introduction into the synthesis are considered as a powerful tool for controlling practically significant characteristics of the metal compounds included in SNPs, such as their accessibility to water molecules and leachability. Special attention is paid to the importance of the identified trends in the management of functional properties such as catalytic activity or acceleration of magnetic relaxation of protons of water molecules, as a prerequisite for the use of such composite SNPs as nanocatalysts or contrast agents in MRI.

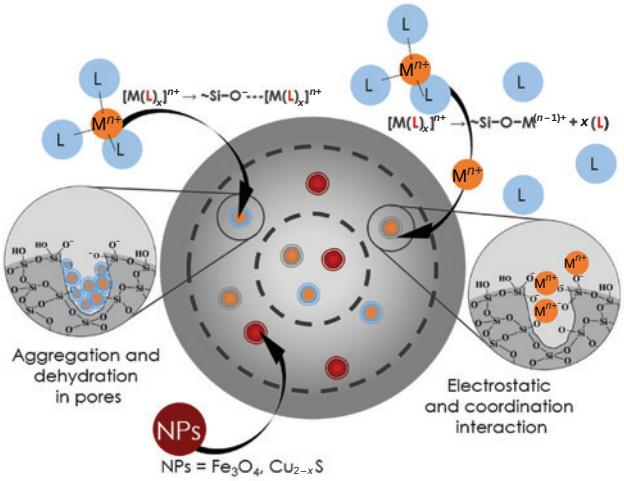

The bibliography includes 112 references.

Keywords: silica nanoparticles, iron oxide, copper sulfide, manganese, contrast agent, catalysis.

Contents

O.D.Bochkova. PhD in Chemistry, Junior Researcher at the Laboratory of Physical Chemistry of Supramolecular Systems of IOPC KSC RAS.
E-mail: o.d.bochkova@mail.ru
Current research interests: silica nanoparticles, contrast agents, catalysis, biosensors, colloidal chemistry, d-metals.

A.S.Stepanov. PhD in Chemistry, Research Fellow at the Laboratory of Physical Chemistry of Supramolecular Systems of IOPC KSC RAS.
E-mail: aleksestepanov@yandex.ru
Current research interests: oxide(sulfide) nanoparticles, colloids, nanoparticulate contrast agents, hyperthermia, photothermia.

A.P.Bebyakina. PhD Student, Junior Research Assistant at the Laboratory of Physical Chemistry of Supramolecular Systems of IOPC KSC RAS.
E-mail: apbebyakina@gmail.com
Current research interests: silica nanoparticles, MRI contrast agents, catalysis, colloidal chemistry, physical chemistry.

A.R.Mustafina. PhD in Chemistry, Chief Researcher at the Laboratory of Physical Chemistry of Supramolecular Systems of IOPC KSC RAS.
E-mail: asiyamust@mail.ru
Current research interests: nanotechnological approaches to the development of contrast and therapeutic agents and biosensors, d(f) metal complexes.

Received 3 April 2026

© 2026 Uspekhi Khimii, ZIOC RAS, Russian Academy of Sciences

1. Introduction

The synthesis of silica nanoparticles (SNPs) has attracted considerable interest due to their wide range of applications in sensing, biology, medicine and agriculture.[1–6] It is worth noting the numerous reviews devoted to the biomedical applications of mesoporous silica nanoparticles (MSNPs) and the main strategies used in their synthesis.[3,7–10] The synthesis and functional properties of mesoporous silica nanostructures with an average pore size greater than 10 nm have been widely discussed. In contrast, similar issues regarding microporous silica nanoarchitectures with pore sizes in the range of 1.3–2.0 nm have received less attention. Both mesoporous and microporous silica nanoarchitectures have their own advantages and disadvantages. For biomedical applications, SNPs with a size of less than 50 nm feature reduced uptake by immune cells.[11] From this point of view, microporous silica nanoarchitectures represent a better choice compared to mesoporous nanoarchitectures. Therefore, this review focuses on microporous nanoarchitectures.

When assessing the influence of size, shape, and porosity of nanoparticles (NPs) on their functional properties, it is important to consider the role of dopants in their composition. Nanoscale metal oxides (sulfides) and metal ions (complexes) deserve special attention as such dopants, as their incorporation into NPs enables the creation of magnetic, paramagnetic, and luminescent nanocomposites.[12–18] In particular, iron oxide and copper sulfide NPs have attracted considerable attention due to their unique functional properties, which are important for biomedicine.[19–24] However, many methods for their synthesis have not yet been sufficiently analyzed and discussed to assess the underlying factors responsible for the incorporation of these dopants into SNPs. Notably, the key challenges encountered in synthesizing both metal oxide/sulfide cores and their silica-coated analogs with highly uniform sizes are similar for a wide range of metals.

The incorporation of metal ions and their complexes into SNPs is another widely used strategy for achieving functional properties such as luminescence, catalytic activity, and paramagnetic enhancement of water proton magnetic relaxation for magnetic resonance imaging (MRI) contrast. It should be noted that achieving the latter functionality is the most challenging task, as it requires obtaining a specific morphology, while the luminescence properties of silica composite nanostructures are less sensitive to morphology due to the transparency of the silica coating. This review focuses on achieving the specific morphology required for effective MRI image contrast enhancement of silica composite nanostructures, with particular emphasis on simple, one-step and one-pot approaches to silica composite nanoarchitectures as an alternative to multistep hydrothermal procedures. The advantages and limitations of these synthesis methods for achieving practical functional properties are discussed below.[25–29] In particular, it was shown that the microporosity of silica nanostructures ensures sufficient accessibility of metal ions for small molecules, including water, when incorporated into the outer silica layer. The variety of d-metal ions and their complexes used as dopants in silica nanostructures is limited in this case to those composite nanostructures that, according to the literature, provide either MRI contrast enhancement or catalytic properties.

This review also examines the synergistic and non-synergistic effects in the synthesis of multifunctional NPs through the combined incorporation of metal compounds and complexes in both nanoscale and molecular forms, as these trends have not yet been sufficiently explored. The known synthesis methods used to obtain such composite SNPs are analyzed in correlation with the fundamental aspects of coordination, interionic and intermolecular interactions associated with the incorporation of both nanosized metal oxides (sulfides) and metal ions (complexes) into the silica matrix.

2. Synthesis of composite SNPs doped with nanosized iron oxides

Iron oxides are the most widely used dopants, which has led to a large number of reported methods for their use in synthesis. This allows us to identify the main regularities of their incorporation into SNPs or silica coatings. It is noteworthy that producing iron oxide NPs with high uniformity in size, shape and phase requires the use of high-temperature precursor decomposition method.[30–34] As a result, the resulting iron oxide-based NPs are hydrophobic due to their oleate-based outer layer. In turn, the ligand exchange of oleates to silanol groups is a key prerequisite for the silica coating of oleate-coated iron oxides.[35–37] There are two main approaches to applying silica coating on hydrophobic NPs: the reverse (water-in-oil) microemulsuion method and Stöber procedure. These methods involve growing the SiO_2 shell by NH_3-catalyzed hydrolysis of tetraethyl orthosilicate (TEOS) followed by polycondensation of hydrolyzed products in alcohol/water media[38] or in water-in-oil microemulsion.[36,39,40]

The application of a silica coating on inorganic hydrophobic NPs by means the reverse microemulsion procedure requires the use of surfactants. The most commonly employed surfactants are Igepal CO-520 and Triton X-100, which possess similar structures and are both polyoxyethylene nonionic surfactants. According to Li and co-workers[35] the use Igepal CO-520 as a surfactant triggers the ligand exchange at the stage of mixing the surfactant with oleate-coated iron oxide NPs in cyclohexane, followed by substitution of absorbed Igepal CO-520 molecules by the hydrolyzed TEOS. It was shown that the interaction between hydrolyzed TEOS and iron oxide NPs is the main driving force behind their transfer to the aqueous phase.[35]

Although the use of the surfactant-free Stöber procedure allows the formation of silica coating on oleate-coated iron oxides, the Fourier-transform infrared spectroscopy (FTIR) spectra of these silica-coated Fe_3O_4 NPs indicate incomplete substitution of oleates by silanol groups on the Fe_3O_4 surface.[41] However, the Stöber procedure was proven to be most successful in producing a silica coating for iron oxides with a hydrophilic surface.[42–44] Thus, a successful application of silica coating on various metal oxide nanocores coated with easily removable molecules is presented.[43–46]

Silica coating of iron oxide cores very often results in the formation of either core-free SNPs or SNPs loaded with several iron oxide cores. It is worth discussing the modifications to the synthesis used by the authors to obtain single-loaded NPs by applying a silica coating on oleate-coated iron oxides using the water-in-oil microemulsion method. The synthesis modifications used for Igepal CO-520 and Triton X-100 are somewhat different, which requires a separate discussion of their use in the microemulsion method. In the case of Igepal, the fractionated addition of TEOS and equal number of iron oxide cores and aqueous nanodomains in water-in-oil mucroemulsions play a decisive role in the formation of high-quality Fe_3O_4@SiO_2 core–shell NPs.[35,47] This can be achieved by the optimization of both iron oxides concentration and low TEOS injection rate. The latter suppresses the homogeneous nucleation of SiO_2 and,

consequently, furnishes single-loaded Fe_3O_4@SiO_2 NPs.[33] Thus, the formation process of single-loaded Fe_3O_4@SiO_2 NPs competes with alternative processes such as aggregation of oleate-coated iron oxide and homogeneous nucleation of SiO_2. The thickness of the silica layer around the magnetic core can be controlled by changing the amounts of TEOS and ammonia used in the synthesis, as well as the reaction time.[32,33,48] Formation of the multicore Fe_3O_4@SiO_2 NPs is explained by aggregation of iron oxide cores prior to coating, and this is typical for the oleate-capped iron oxide cores with the size below 10 nm.[33] However, the formation of double- and multi-core NPs can occur due to too rapid addition of TEOS to the synthetic mixture, when some amount of TEOS undergoes homogeneous nucleation.[49,50] The synthesis of high-quality single-core, monodisperse Fe_3O_4@SiO_2 core-shell NPs has been accomplished using an approach similar to those used in numerous studies, though the authors did not provide the specific details of the coating procedure.[51,52]

Similar to the method using Igepal CO-520, when using the Triton X-100-based microemulsion method, the high addition rate of TEOS should be responsible for the formation of coreless SNPs during the silica coating of oleate-capped iron oxides. However, when TEOS is added after all other reactants in the synthesis process, a minor amount of core-free SNPs is formed compared to single-loaded SNPs even at a relatively high TEOS addition rate (1 mL min^{-1}).[53] The above procedure facilitates the formation of single-loaded SNPs when the size of oleate-coated iron oxides is 12.8 nm.[53] Multicore SNPs are produced by incorporating small (6 nm) oleate-capped iron oxide NPs into SNPs, and such multicore loading results in a higher contrast effect in MRI compared to single-loaded SNPs.[54] The multicore SNPs are formed as a result of a higher degree of aggregation of iron oxide NPs smaller than 10 nm due to their higher surface Gibbs free energy compared to larger iron oxide NPs.[54]

As noted above, the application of silica coatings to oleate-capped iron oxide NPs is facilitated by nonionic surfactants, as they remove surface oleates. However, it should be noted that surface oleates can be removed from iron oxide NPs through the coordination or electrostatic binding of oleates to metal ions or metal complexes. In particular, the combined use of the differently sized iron oxides and Mn^{2+} ions in the synthesis leads to a significant synergistic effect, facilitating the incorporation of both Mn^{2+} ions and iron oxides into SNPs.[55] This synergistic effect can be explained by complex formation between Mn^{2+} ions with oleates removed from oleate-capped iron oxide NPs.[55] However, such effect is insignificant when iron oxide NPs of different sizes are introduced in combination with the thermodynamically stable Gd^{3+} complex.[53,54] It is worth mentioning another intriguing example of the codoping effect on the iron oxides incorporation. This effect is evident from a comparative analysis of the incorporation of 24 and 17 nm oleate-capped iron oxides into SNPs by microemulsion synthesis, where the former NPs are introduced alone and the latter are introduced in combination with the $[Ru(bpy)_3]^{2+}$ (bpy is 2,2′-bipyridine) complex.[19,56] Both syntheses were carried out in a similar manner at a high TEOS addition rate, although the loading of 24 nm core SNPs is less efficient than that of their smaller counterparts.[19,56] In particular, the formation of singly loaded SNPs is accompanied by the formation of unloaded and multiply loaded NPs in the case of incorporation of 24 nm sized iron oxides without this complex.[56] However, the formation of single-core SNPs becomes predominant in the case of the codoping of 17 nm iron oxide particles with $[Ru(bpy)_3]Cl_2$.[19] This may be due to some removal of surface oleates due to ionic binding of oleates to these complex cations. Figure 1 schematically demonstrates the above-described effects of both non-ionic surfactants and co-dopants as the factors promoting the silica-coating of iron oxide species.

The data presented in Table 1 demonstrate the key synthetic characteristics known from the literature that are responsible for the formation of monodisperse iron oxide-loaded NPs when the latter are introduced into the reaction mixture as oleate-coated NPs.

Encapsulation of hydrophobic iron oxide NPs into silica matrix *via* the Stöber procedure can be facilitated by modifying it with positively charged surfactants such as CTAB.[20,59] The main role of CTAB was shown to involve the transfer of hydrophobic iron oxide NPs to the aqueous phase.[20,59] Therefore, the water dispersible CTAB-modified iron oxide NPs obtained in the first stage of synthesis provide the basis for the formation of high-quality silica-coated iron oxide NPs.[20,59] However, CTAB also serves as a template for the formation of a mesoporous silica layer on the surface of iron oxide NPs.[59] This synthetic strategy allows the formation of spherical, uniform-sized and single-loaded core-shell nanoparticles after removing CTAB molecules from silica by refluxing the SNPs in acidic ethanol solutions. Notably, the synthetic strategy using CTAB was successfully used to deposit silica coating on CdTe nanocores.[21]

3. Synthesis of composite SNPs doped with nanosized copper sulfides

Copper(I)-based chalcogenide compounds mainly represented by copper sulfides $Cu_{2-x}S$ have gained great attention as

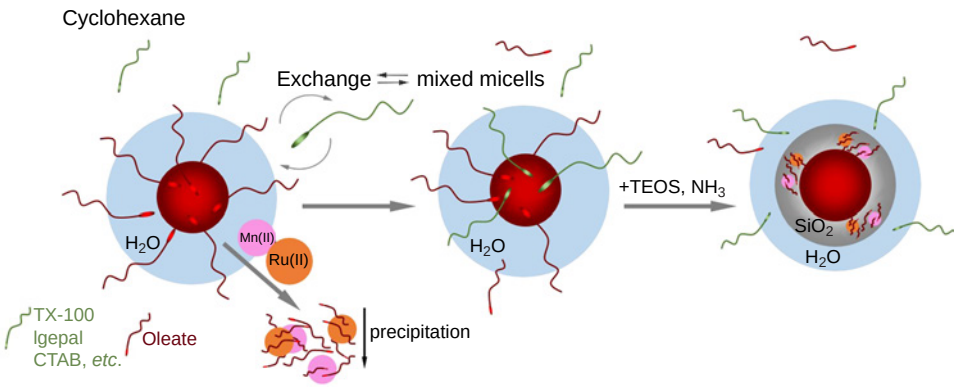

Figure 1. Schematic presentation of the interactions facilitating removal of the surface oleates from oleate-capped iron oxide NPs. TX-100 is Triton X-100, CTAB is cetyltrimethylammonium bromide.

Table 1. Methods and reaction conditions for the synthesis of silica-coated iron oxides, and characteristics of the resulting nanoparticles.

Method of synthesis	Surf.	Base	R	Size, nm	Shape	State	Properties	Ref.
Reverse microemulsion	Igepal-520	NH_3	2.48	20	Spheres	Monodisperse	–	35
Reverse microemulsion	Igepal-520	NH_3	1.11	45	Spheres	Monodisperse	High relaxivities	33
Reverse microemulsion	Igepal-520	NH_3	0.96	30	Spheres	Moniodisperse	Magnetic imaging	57
Reverse microemulsion	Triton X-100	NH_3	0.79	113	Spheres, quasi-spheres	More polydisperse, core-free NPs	High relaxivities along with high specific adsorption rate	53
Reverse microemulsion	Triton X-100	NH_3	0.29	90	Spheres	Monodisperse, core-free NPs	High specific adsorption rate	56
Reverse microemulsion	Triton X-100	NH_3	0.29	80	Spheres	Monodisperse, core-free NPs	Enhancing the neuronal activity of motoneurons	19
Reverse microemulsion	Triton X-100	NH_3	0.77	–	Spheres, quasi-spheres	More polydisperse, fused NPs	High relaxivities	58
Sol–gel method	Igepal-520	NH_3	Not specified	35	Quasi-speres	Polydisperse	–	47
Base-catalyzed sol–gel reaction	Igepal-520	NH_3	Not specified	50	Spheres	Monodisperse	High relaxivities	51
Sol–gel reaction microemlsion	Igepal-520	NH_3	3.19	20	Spheres	Monodisperse, minor amount of core-free NPs	High relaxivities	52
CTAB-facilitated synthesis	CTAB	NaOH	0.5	95	Spheres	Monodisperse	High relaxivities	59
CTAB-facilitated synthesis	CTAB	NaOH	4.57	105	Spheres	Monodisperse	Magnetic resonance, fluorescent imaging	20
CTAB-facilitated synthesis	CTAB	NaOH	0.02	100	Spheres, quasi-spheres	Monodisperse	Imaging, drug delivery, theurapetic applications	21
Reverse microemulsion	Igepal-520	NH_3	1.105	30	Spheres	Monodisperse	High relaxivities	49
Reverse microemulsion	Igepal-520	NH_3	0.93	50	Spheres	Monodisperse	High relaxivities	48
Stöber process	–	–	–	153	Qquasi-spheres	Monodisperse	High relaxivities	42

Notes. A dash means no data is available on specific applications of the prepared nanoparticles. Surf. is surfactant, R is the ratio of the concentrations of bases and surfactants.

promising basis of chemodynamic and photothermal agents, which can be considered as very promising therapeutic agents.[60,61] The use of high-temperature liquid phase synthesis is the best choice to control both the size and the crystalline phase of the $Cu_{2-x}S$ nanocores, although they should be hydrophilized for further biomedical applications.[62] Silica coating of oleate-oleylamine-capped copper sulfides is a good strategy to combine their photothermal and chemodynamic acitivities with luminescent properties.[63] However, successful silica coating of oleate-oleylamine coated copper sulfides is achieved by desorbing their hydrophobic coating in acidified solutions as a preliminary step before silica coating.[63,64] The purpose of this preliminary step is to facilitate the coordination of silanol groups on the surface of copper sulfides.

However, not only the difficulties of replacing oleate and oleylamine ligands with hydrolyzed TEOS on the surface of such copper sulfide cores, but also their specific aggregation in aqueous media is a serious obstacle to the monocore incorporation of copper sulfides into SNPs by the water-in-oil microemulsion procedure. The above-mentioned aggregation specificity of oleate-oleylamine capped copper sulfides is manifested in their ability to form negatively charged aggregates, which stems from the ability of oleates to contribute to the hydrophobic layer of $Cu_{2-x}S$ and to serve as hydrophilic agents due to the Janus-like localization, schematically shown in Fig. 2.[22–24] Thus, the electrostatic repulsion between oleate-oleylamine-coated copper sulfides and the *in situ* formed silica seeds should be considered as the main factor limiting the formation of silica-coated copper sulfide particles. This limitation can be avoided by the recovery of oleate-oleylamine-capped copper sulfides by cationic

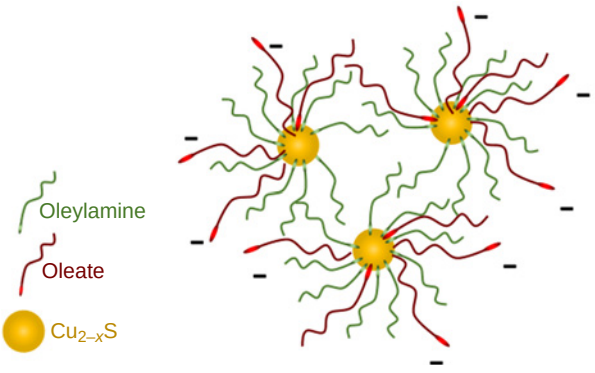

Figure 2. Schematic representation of negatively charged aggregates formed from copper sulfides modified with oleate and oleylamine in an aqueous medium.

surfactants.[22,24,65–67] A similar, but less pronounced effect is observed with the simultaneous introduction of oleate-oleylamine-capped $Cu_{1.75}S$ cores and the cationic $[Ru(bpy)_3]^{2+}$ complex.[23,24] These composite NPs suffer from insufficient loading uniformity since they are mainly represented by multi-core SNPs. The roles of cationic surfactants and the cationic complex are not limited to recharging the surface of oleate-oleylamine-capped copper sulfide, but are also associated with the removal of oleates due to their interaction with cationic surfactants or $[Ru(bpy)_3]^{2+}$. Although both of the above cationic compounds promote the interaction of both hydrolyzed TEOS and *in situ* formed silica nuclei with copper sulfides, the beneficial effect of the cationic surfactant is superior to that of the cationic complex.[22,65]

However, additional synthetic tricks as, *e.g.*, shown in Refs 65, 66, 68, are required to limit the aggregation of the CTAB-recovered $Cu_{2-x}S$ cores. In particular, Znang *et al*.[68] developed a procedure that allows the preparation of spherical monodisperse core–shell SNs loaded with $Cu_{1.8}S$ of 17.58 nm size, without any core-free SNPs. Notably, the use of uncoated calcined copper-based cores such as CuO does not provide their uniform coating with silica.[69] *Vice versa*, this approach results in the formation of core–shell SNPs that vary significantly in size, shape and loading, since the original uncoated cores suffer from high polydispersity and aggregation.[69]

The above trends indicate the key role of removing the oleate-oleylamine coating from the surface of copper sulfide cores for subsequent silica coating, both due to electrostatic attraction and due to formation of coordination bonds between deprotonated silanol groups and metal ions on the surface of nanosized metal oxides (sulfides). Table 2 summarizes data on the successful synthesis of copper sulfide-loaded nanoparticles, in which loading is facilitated either by co-doping additives or cationic surfactants.

4. Doping of SNPs with metal ions

Before discussing the synthesis methods used to load SNPs with metal ions and complexes, it is important to explain the primary driving forces behind this process. In the case of metal ions, loading occurs through the entrapment of metal ions within the silica pores, both through the electrostatic attraction of the metal ions to the $Si–O^-$ groups and through their coordination bonds. Interestingly, these interactions are particularly enhanced when they occur within the confined space of silica pores.[70] In this regard, Ahkam *et al*.[58] showed that when the Co content in the SiO_2 phase does not excees 2%, a uniform distribution of Co^{2+} ions in SNs prevails due to the formation of Si–O–Co coordination bonds. Formation of coordination Si–O–Mn bonds is also highlighted as a key reason for the loading of SNs with Mn^{2+} ions.[25,71,72] It is noteworthy that the formation of coordination bonds is the sole driving force for the incorporation of metal ions into SNs only when the synthesis is carried out under weakly acidic conditions.[73] Moreover, the introduced Co^{2+} ions significantly disrupt the structure of SiO_2 due to the larger atomic radius of Co^{2+} compared to that of Si^{4+}, which is manifested in a larger pore size. However, the use of alkaline conditions for nanoparticle production is much more common in terms of controlling the size, shape, and homogeneity of the SNPs.[40,74,75] Notably, these conditions promote the coordination of metal ions with silanol groups but cause hydrolysis of the metal ions.[76] At high concentrations of Co^{2+} and Mn^{2+} salts, this leads to the formation of metal oxides as a separate phase.[26,58,77]

The conditions of alkali-catalyzed hydrolysis of TEOS induce the oxidation of Mn^{2+} to $Mn^{3(4)+}$ (see Refs 25–27, 78, 79), which reduces the ability of Mn-containing SNPs to increase the rate of magnetic relaxation of protons in water molecules. This drawback can be avoided by using multistage hydrothermal procedures based on the thermodynamically favorable reduction of oxidized manganese ions in an additional synthesis step.[28,71,72,80–82] It should be noted that the use of Si–O–Mn coordination bonds is quite effective[83] for incorporating of Mn^{2+} ions into NPs and for preventing hydrolytic and oxidative transformations of Mn^{2+} (see Ref. 84). Thus, the synthesis conditions can be adjusted to promote the formation of Si–O–Mn coordination bonds rather than hydrolysis and oxidative transformation of Mn^{2+} ions. Nevertheless, the latter processes cannot be ruled out entirely. This can be achieved both in ethanol-based environment in the Stöber method and in the aqueous nanodroplet using the water-in-oil microemulsion

Table 2. Method of synthesis, reaction conditions, and characteristics of the resulting nanoparticles.

Type of NPs	Method of synthesis	Surf.	Base	R	Size, nm	Shape	State	Properties	Ref.
$Cu_{2-x}S@SiO_2@[Ru(bpy)_3]^{2+}$	Reverse microemulsion	Triton X-100	NH_3	0.03	50	Spheres	Aggregated, polydisperse	Photothermal, chemo-dynamic therapy	24
$Cu_{2-x}S@SiO_2@[Ru(bpy)_3]^{2+}$	Reverse microemulsion	Triton X-100	NH_3	0.297	60	Spheres	Aggregated, polydisperse	Chemodynamic therapy	23
$Cu_{2-x}S@SiO_2–NH_2$	Reverse microemulsion	CTAB	NaOH	11	40	Spheres	Aggregated, polydisperse	Photothermal and chemodynamic	22
$Cu_{2-x}S@mSiO_2$	Hydrolysis of TEOS by NaOH	CTAB	NaOH	0.96	65	Spheres	Monodisperse	Photothermia	65
$Cu_8S_5@SiO_2@Er_2O_3$	Stöber method	–	NH_3	–	8	Spheres	Monodisperse	Plasmon-enhanced up-conversion luminescence	63
$Cu_{2-x}S@mSiO_2$	Hydrolysis of TEOS by NaOH	CTAB	NaOH	–	–	Spheres	Monodisperse	Luminescence	66
$CuO@mSiO_2$	Stöber method	–	NH_3	–	–	Spheres, quasi-spheres, worm-like	Aggregated	–	69

Notes. A dash means no data is available.

method,[26] although the SNPs synthesized by both methods are loaded with both Mn^{2+} and its oxidized forms.

The contrast effect of SNPs loaded with Mn^{2+} using typical water-in-oil microemulsion and Stöber methods[25,26,84] is rather high, despite the admixture of oxidized forms of Mn^{2+}. However, the microemulsion method has some advantages over the Stöber process,[26] which include a higher Mn content in SNPs achieved upon the Mn-loading using microemulsion method compared to the Stöber method.[26] A similar trend is observed for other metal ions, as demonstrated by comparing the Co content when loading Co^{2+} ions using the Stöber and microemulsion methods.[78] To clarify this, it should be noted that, in the microemulsion method, metal ions are concentrated in aqueous nanodroplets. In contrast, such concentration is not possible in the Stöber method, as illustrated schematically in Fig. 3. It is also noteworthy that introduction of Co^{2+} ions into SNPs by the Stöber method leads to their tetrahedral inner-sphere symmetry with a lower hydration number compared to Co^{2+} ions with octahedral symmetry introduced into SNPs by the microemulsion method.[78] Since the higher hydration number of paramagnetic ions promotes their ability to accelerate the magnetic relaxation of water protons,[79] this trend can also be considered as an additional reason for the advantage of the microemulsion method over the Stöber process in the synthesis of Mn-loaded SNPs. The third advantage of the microemulsion procedure over the Stöber method is the higher microporosity of the SNPs obtained by the former method, which is due to the removal of non-ionic surfactants used in the microemulsion method.[27,28] This microporosity facilitates the diffusion of water molecules through the silica matrix, enhancing the hydration of Mn^{2+} ions embedded in this matrix, which in turn allows for enhanced exchange of water molecules in the inner sphere of paramagnetic ions, which increases their contrast in MRI.[13,80,81,85]

Thus, SNPs loaded with various metal ions represent a promising basis for use as catalytic or contrast agents for MRI.[26,82,86–89] The data presented in Table 3 demonstrate the key features of the synthesis methods used to incorporate manganese and cobalt ions into SNPs, indicating both the oxidation states of the metal ions within the SNPs and the preferred zones of their localization within these SNPs. However, great number of functional properties of SNPs cannot be achieved by their loading with metal ions. In particular, to enhance the fluorescence of SNPs or improve their contrast for MRI, metal complexes rather than metal ions should be included in the SNPs composition.

5. Doping of metal complexes into SNs

Incorporating of metal complexes into SNPs is an alternative to grafting them onto the SNPs surface. Although these types of incorporation of metal complexes into SNPs are aimed at achieving similar functional capabilities, the different results of their use should be considered. In particular, the inclusion of metal complexes into silica matrix of the SNPs keeps their surface silanol groups open for further PEGylation or conjugation with biomolecules.[27,28] Considering the excellent examples of grafting metal complexes through these groups, it can be noted that the stability of such surface complexes depends solely on the coordination ability of the ligands grafted to the surface.[96–102] However, the literature does not adequately cover either the driving forces behind the incorporation of metal complexes into

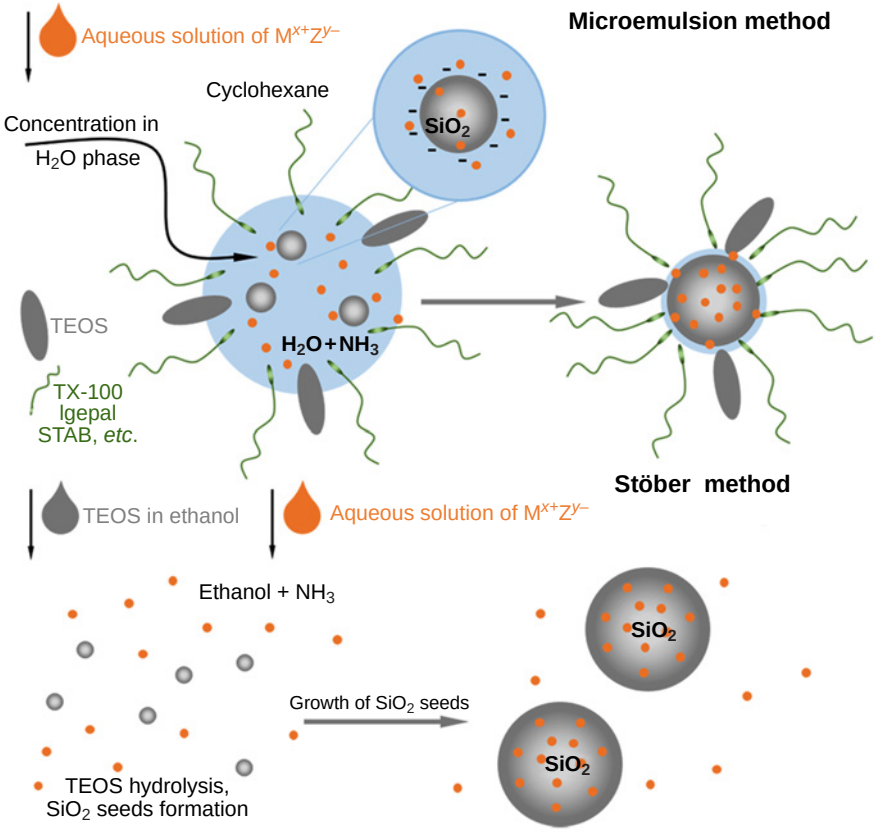

Figure 3. A schematic illustration of different concentrations of metal compounds in silica nanoparticles using the water-in-oil microemulsion and Stöber methods.

Table 3. Methods for incorporating metal ions and complexes into SNPs, oxidation states of metal ions and preferred zones of their localization in SNPs. Functional characteristics of the resulting SNPs.

Metal compound: starting/ in SNs	Method of synthesis	Loading zone of SNPs	Oxidation state of a metal ion in SNPs	Functional characteristics of SNPs	Ref.
H_2tpada–Mn^{II} complex (C1)/ H_2tpada–Mn^{II} complex (C1)	Reverse microemulsion	Core	2^+	High relaxivity. for C1: r_1 = 2.75 mM^{-1} s^{-1}; for C1@SiO_2–NH_2–NP: r_1 = 12.75 mM^{-1} s^{-1}; for C1@SiO_2–FA–NP: r_1 = 21.45 mM^{-1} s^{-1} in H_2O, r_1 = 40.97 mM^{-1} s^{-1} in the presence of 0.67 mM of BSA	27
H_2PyDPA–Mn^{II}-complex/ H_2PyDPA–Mn^{II}-complex	Reverse microemulsion	Core	2^+	Good relaxivity. r_1 = 8.46 mM^{-1} s^{-1} r_2 = 33.15 mM^{-1} s^{-1} at pH = 7.4, 25°C and 1.41 T	90, 91
$MnCl_2 \cdot 4H_2O$/Mn–O–Si	One-pot Stöber method	Uniform distribution	2^+, 3^+, 4^+	r_1 = 1.07 mM^{-1} s^{-1} (pH = 7.4, GSH = 0 mM), r_1 = 2.42 mM^{-1} s^{-1} (pH = 5.0, GSH = 0 mM), r_1 = 5.91 mM^{-1} s^{-1} (pH = 7.4, GSH = 10 mM) Efficient antitumor activity	25
$KMnO_4$/MnO_2	Modified Stöber method	Shell	4^+	r_1 = 0.116 mM^{-1} s^{-1} at pH 7.4, r_1 = 0.741 mM^{-1} s^{-1} at pH5.5 , r_1 = 8.607 mM^{-1} s^{-1} at 10 mM GSH and pH 5.5	92, 93
$MnNO_3 \cdot 6H_2O$/Mn–O–Si	Reverse microemulsion, Stöber method	Uniform distribution	2^+, 3^+, 4^+	Good relaxivity. r_1 = 13.8 mM^{-1} s^{-1} r_2 = 16.9 mM^{-1} s^{-1}	26
Mn(OX)/Mn(OX)	Reverse microemulsion	Shell	2^+	High relaxivity. r_1 = 55.1 mM^{-1} s^{-1} r_2 = 67.5 mM^{-1} s^{-1}	28
$Mn(OL)_2$/$Mn(OL)_2$	Reverse microemulsion	Shell	2^+	High relaxivity. r_1 = 28.5 mM^{-1} s^{-1} r_2 = 34.1 mM^{-1} s^{-1}	28
$(CoCl_2 \cdot 6H_2O)$/Co_2O_3	Sol–gel method	Uniform distribution	2^+, 3^+	No specific applications	58
$(Co(NO_3)_2 \cdot 6H_2O$/Co_3O_4	Sol–gel method	Uniform distribution	2^+, 3^+	Peroxidase-like activities toward the reduction of hydrogen peroxide and oxidation of 2,2′-azino-bis(3-ethylbenzothiazoline-6-sulfonic acid) diammonium salt as a chromogenic substrate	77
$Co(NO_3)_2 \cdot 6H_2O$ and $[Co(bpy)_3]^{2+}$ / Co-O-Si	Reverse microemulsion, Stöber method	Uniform distribution	2^+	Electrochemical response on glyphosate	78
$[Co(bpy)_3]^{3+}$/$[Co(bpy)_3]^{3+}$	Reverse microemulsion	Uniform distribution	3^+	Electrochemical DNA probe for high sensitivity DNA hybridization analysis.	94
$[Co(bpy)_3]^{3+}$/$[Co(bpy)_3]^{3+}$	Reverse microemulsion, Stöber method	Uniform distribution	3^+	Catalyst for oxidative CH/NH cross-coupling reaction	95
$Co(NO_3)_2 \cdot 6H_2O$/ Co_3O_4 (Si–O–Co)	Sol–gel method	Uniform distribution	2^+	Catalyst for liquid-phase oxidation of phenol with H_2O_2	73

Notes. Tpada is 6,6′-((pyridin-2-ylmethylazanediyl)bis(methylene))dipicolinic acid, PyDPA is 6,6′-(((2-carboxyethyl)azanediyl)bis(methylene)) dipicolinic acid, OX is oxalate, OL is oleate, r is relaxivity, GSH is glutathione, BSA is bovine serum albumin, C1 is H_2tpada–Mn^{II} complex, C1@SiO_2–NH_2–NP is aminomodified silica nanoparticles doped with C1 complex, C1@SiO_2–FA–NP is folate-modified silica nanoparticles doped with C1 complex.

SNPs or the positive results of such incorporation. This review therefore focuses on these issues.

Of special note is the $[Ru(bpy)_3]^{2+}$ complex, which is perhaps the first and most frequently incorporated complex into SNs.[40, 103, 104] The electrostatic attraction of this complex to the silica surface is the widely recognized reason for its inclusion in SNPs. Another reason for the widespread use of this complex that has already been noted, is its kinetic inertness, which prevents hydrolytic transformation of the complex when it is included in SNPs. Therefore, such kinetically inert complexes as $[Ru(bpy)_3]^{2+}$, $[Ru(phen)_3]^{2+}$ (phen is 1,10-phenanthroline), $[Co(bpy)_3]^{3+}$ were already included into the SNPs.[27, 29, 90, 91] Incorporation of these complexes into SNPs without their transformation during the synthesis process can be achieved by simply introducing them into the synthetic mixture (Fig. 4). However, labile Mn^{2+} complexes can be incorporated into SNPs without detectable oxidation only if their thermodynamic stability is high enough to exclude their hydrolytic transformations.[27, 28] In the case of labile Co^{2+} complexes, even tris-chelated Co^{2+} complexes with high thermodynamic stability, such as $[Co(bpy)_3]^{2+}$, exhibit complete degradation during synthesis due to the formation of Si–O–Co coordination

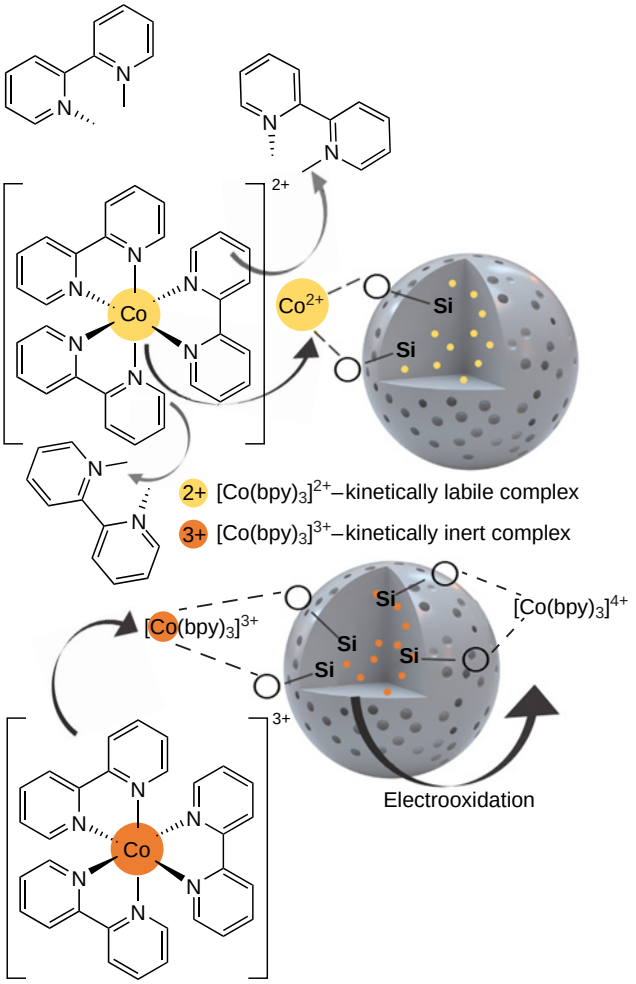

Figure 4. Schematic representation of the incorporation of kinetically labile and inert complexes into silica nanoparticles and the possible electrochemical Co^{3+}/Co^{4+} transformation.

bonds[78] (see Fig. 4). Notably, the thermodynamic advantage of coordination bonds with $Si–O^-$ groups is higher for Co^{2+} compared to other d-metal ions. This is confirmed by the less pronounced degradation of similar Ni^{2+} complexes during the synthesis of nickel-containing SNPs.[95]

Notably, the confined complex may exhibit leaching from SNPs caused by the concentration gradient. In the context of biomedical application of the SNPs loaded with luminescent or paramagnetic metal complexes as cellular markers or MRI contrast agents, this leaching should be minimized. In particular, the leaching of such complexes is usually associated with both their toxicity and changes or deterioration of the functional properties of the composite SNPs. Indeed, independent flux of the complex from the SNPs reduces their ability to label cells, and the contrast ability of paramagnetic ions also decreases after their removal from the composite SNPs. Notably, an electrostatic attraction of the $[Ru(bpy)_3]^{2+}$ complex to deprotonated silanol groups at the SNPs surface somewhat retards but not limit the complex leaching. This is clearly demonstrated by comparing the leaching of $[Ru(bpy)_3]^{2+}$ from nanoparticles loaded with $[Ru(bpy)_3]^{2+}$ alone and those loaded with both this complex and the anionic Mn^{2+} complex with *p*-sulfonatothiacalix[4]arene ligand.[105] This trend is also well illustrated by studies that have shown the leaching of structurally similar complexes with different solubilities in water from SNPs synthesized by the same microemulsion method.[105,106] These complexes are based on the well-known water-soluble ligand *p*-sulfonatothiacalix[4]-arene, which forms $Gd(Tb)^{3+}$ complexes with limited water solubility, while its Mn^{2+} complex features higher water solubility compared to $Gd(Tb)^{3+}$ complexes.[105–109] Of special note is the study,[70] which highlights the tendency that has a great impact on the capture of ions and ionic complexes by silica pores. The dehydration of ionic compounds caused by the confinement of silica pores enhances the ion-pairing of these ions with counter-ions,[70] which is an additional reason for their effective capture in the pores of SNPs. Dehydration of the complexes embedded in a silica matrix is well illustrated by the work.[110] There, nitrosyl Ru^{II} complexes embedded in SNPs exhibit a low capacity for photoinduced NO release due to their insufficient hydration, since photoinduced NO release corresponds to equilibrium (1).

$$[Ru^{II}NO^+(L)_4(X)]^{2+} + h\nu + H_2O \longrightarrow [Ru^{III}(L)_4(X)(H_2O)]^{2+} + NO^0 \quad (1)$$

The specific microenvironment of metal complexes in silica pores affects not only their hydration state but also their redox activity. This has been demonstrated for the $[Co(bpy)_3]^{3+}$ complex, which, when incorporated into NPs synthesized by various methods, exhibits oxidation peaks at reasonable potential values associated with the Co^{3+}/Co^{4+} oxidation process.[95] This process is impossible for $[Co(bpy)_3]X_3$ in solution or solid state, but is favorable for complexes incorporated into SNPs, with the greatest favorability observed for nanoparticles synthesized by the microemulsion method, as schematically demonstrated in Fig. 4. The catalytic properties of the cobalt(III) trisbipyridyl complex are significantly improved when it is incorporated into SNPs obtained by the reverse microemulsion method compared to those synthesized by the Stöber method. The high microporosity of the silica surface of SNPs obtained by the microemulsion method can be considered as a factor facilitating the accessibility of the Co^{3+} metal sites to reagents.[95]

The identified relationships open the possibility of loading SNPs with metal ions using anions, which convert them into water-insoluble compounds. The use of oxalate as a concomitant additive significantly limits the oxidation of Mn^{2+} ions during their inclusion into SNPs.[28] Furthermore, the functional properties of composite microporous SNPs can be optimized by modifying their nanoarchitecture. It has already been shown that loading of Mn^{2+} into an outer layer of SNPs has a key impact on obtaining such important functional property as paramagnetic enhancement of magnetic relaxation of water protons, which is necessary to achieve the contrast effect in MRI.[12,85,111] The predominant concentration of metal-based additives, in both the core and outer layer of the silica nanoarchitecture, can be achieved by stepwise introduction of Mn^{2+} ions and their accompanying additives during the microemulsion synthesis method.[28,78,111,112] Table 3 presents successful examples of the incorporation of cobalt and manganese complexes to achieve efficient magnetic relaxation or catalytic performance.

The aforementioned synergistic effect of Mn^{2+} ions on the silica coating of oleate-coated iron oxides is accompanied by complete limitation of oxidative transformations of Mn^{2+} due to the formation of water-insoluble manganese oleate.[55] This was confirmed by further studies of the effects of oleates and oxalates on Mn^{2+} incorporation into SNs.[28] In this regard, the reported synergistic effect of $[Ru(bpy)_3]^{2+}$, Mn^{2+} and oxalate anions[112] also arises through cooperative ionic binding within silica pores. Figure 5 shows the predominant concentration of ionic

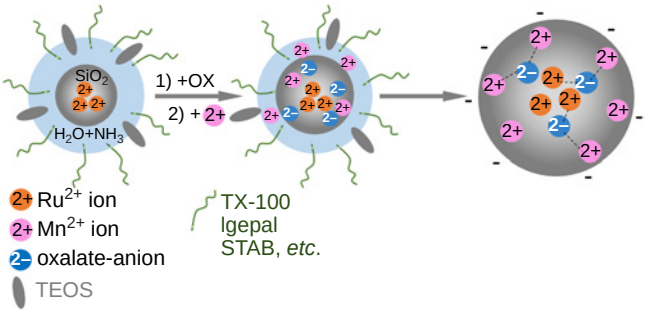

Figure 5. Schematic representation of the origin of the synergistic effect of $[Ru(bpy)_3]^{2+}$ as a co-doping agent in oxalate-induced Mn^{2+} incorporation into SNPs. Ox is oxalate-anion.

compounds with opposite charges in different SNs zones, due to their stepwise introduction, which prevents their leaching and facilitates the inclusion of Mn^{2+} ions as a third component.

It should also be noted that the functional properties of the complexes change after encapsulation in a silica matrix due to coordination transformations occurring during synthesis, which is well illustrated by the kinetically labile and insufficiently stable Co^{2+} and Mn^{2+} complexes, as schematically shown in Fig. 4. However, even if such transformations are minimized, the functional properties of complexes encapsulated in silica pores significantly change under the influence of a silica environment. This change is due to the dehydration of such complexes, which is more pronounced for complexes that are incorporated into the core of SNPs than for those concentrated in the outer silica layer.[26,105,107] In the case of Mn^{2+} complexes, their localization in the core or in the outer layer of silica nanoparticles significantly affects their ability to accelerate the magnetic relaxation of protons in water molecules.[26,105] It is also worth noting the significant role of the variously modified microemulsion synthetic technique in the synthesis of functional composite SNPs.

6. Conclusion

The practical significance of SNPs loaded with metal compounds or complexes has provoked interest in the fundamental transformations these compounds or complexes undergo when incorporated into the silica matrix. An analysis of the literature shows that coordination and electrostatic bonding are the main driving forces behind the incorporation of metal ions, complexes and nanoscale metal oxides/sulfides. Thus, when metal oxides/sulfides are used in the synthesis in the form of oleate-coated NPs, the removal of oleate becomes an important factor in facilitating the coordination and electrostatic interactions between the hydrolyzed TEOS and the silica cores formed *in situ* with the metal ions on the surface of the metal oxides/sulfides. It should be noted that the same driving forces are fundamental when incorporating both metal ions and complexes, allowing for the production of composite SNPs with diverse functional properties. The results presented in the literature demonstrate that the significant coordination capacity of surface silanol groups and the specific environment of silica pores are key drivers of changes in the internal and/or external spheres of metal ions. Understanding these processes is essential if they are to be used as a tool for modifying the functional properties of composite SNPs. The correct choice of ligand was shown to facilitate both the incorporation of metal ions into SNPs and the modification of their functionality.

A comparative analysis of the two most widely used synthesis methods, *viz*., the Stöber process and the water-in-oil microemulsion method, indicates that the latter is more effective in producing SNPs with higher metal content and greater surface microporosity. This is particularly important for optimizing the functional properties of SNPs, such as accelerating the magnetic relaxation of water molecules or interactions with reagents, which is necessary for their use as contrast agents for MRI or as nanocatalysts.

7. List of abbreviations

bpy — 2,2′-bipyridine;
CTAB — cetyltrimethylammonium bromide;
FTIR — Fourier-transform infrared spectroscopy;
MRI — magnetic resonance imaging;
MSNP — mesoporous silica nanoparticle;
NP — nanoparticle;
phen — 1,10-phenanthroline;
SNP — silica nanoparticle;
TEOS — tetraethyl orthosilicate.

8. References

1. A.S.Taleghani, A.T.Nakhjiri, M.J.Khakzad, S.M.Rezayat, P.Ebrahimnejad, A.Heydarinasab, A.Akbarzadeh, A.Marjani. *J. Mol. Liq.*, **328**, 115417 (2021); https://doi.org/10.1016/j.molliq.2021.115417
2. P.G.Jeelani, P.Mulay, R.Venkat, C.Ramalingam. *Silicon*, **12** (6), 1337 (2020); https://doi.org/10.1007/s12633-019-00229-y
3. J.G.Croissant, K.S.Butler, J.I.Zink, C.J.Brinker. *Nat. Rev. Mater.*, **5** (12), 886 (2020); https://doi.org/10.1038/s41578-020-0230-0
4. F.Akhter, A.A.Rao, M.N.Abbasi, S.A.Wahocho, M.A.Mallah, H.Anees-ur-Rehman, Z.A.Chandio. *Silicon*, **14** (14), 8295 (2022); https://doi.org/10.1007/s12633-021-01611-5
5. T.I.Janjua, Y.Cao, F.Kleitz, M.Linden, C.Yu, A.Popat. *Adv. Drug Deliv. Rev.*, **203**, 115115 (2023); https://doi.org/10.1016/j.addr.2023.115115
6. I.A.Rahman, V.Padavettan. *J. Nanomater.*, **2012**, 1 (2012); https://doi.org/10.1155/2012/132424
7. R.Narayan, U.Y.Nayak, A.M.Raichur, S.Garg. *Pharmaceutics*, **10** (3), 118 (2018); https://doi.org/10.3390/pharmaceutics10030118
8. C.Bharti, U.Nagaich, A.Pal, N.Gulati. *Int. J. Pharm. Invest.*, **5** (3), 124 (2015); https://doi.org/10.4103/2230-973X.160844
9. S.-H.Wu, C.-Y.Mou, H.-P.Lin. *Chem. Soc. Rev.*, **42** (9), 3862 (2013); https://doi.org/10.1039/c3cs35405a
10. A.Mehmood, H.Ghafar, S.Yaqoob, U.F.Gohar, B.Ahmad. *J. Develop. Drugs*, **06** (02), 174 (2017); https://doi.org/10.4172/2329-6631.1000174
11. S.M.Narum, T.Le, D.P.Le, J.C.Lee, N.D.Donahue, W.Yang, S.Wilhelm. In *Nanoparticles for Biomedical Applications*; *Passive Targeting in Nanomedicine: Fundamental Concepts, Body Interactions, and Clinical Potential*. (Eds E.Ji Chung, L.Leon, C.Rinaldi) (Elsevier, 2020). Ch. 4. P. 37; https://doi.org/10.1016/B978-0-12-816662-8.00004-7
12. L.Tei, M.Botta, C.F.G.C.Geraldes. *Acta Biomater.*, **207**, 468 (2025); https://doi.org/10.1016/j.actbio.2025.05.058
13. G.Deka, R.Mallik, I.Sk, C.Mukherjee. *ACS Appl. Bio Mater.*, **8** (6), 4592 (2025); https://doi.org/10.1021/acsabm.5c00747
14. S.F.O.Aboushoushah. *J. Science: Adv. Mater. Devices*, **10** (2), 100875 (2025); https://doi.org/10.1016/j.jsamd.2025.100875
15. Y.D.Gupta, S.Bhandary. *WIREs Nanomed Nanobiotechnol.*, **17** (3), e70023 (2025); https://doi.org/10.1002/wnan.70023
16. I.C.B.Pires, I.A.S.Filho, C.T.T.Nunes, S.A.Junior, J.M.Mathis. *J. Nanopart. Res.*, **27** (7), 181 (2025); https://doi.org/10.1007/s11051-025-06347-6

17. Z.Sun, X.Li. *J. Mater. Chem. B*, **13** (6), 1935 (2025); https://doi.org/10.1039/D4TB01822B
18. B.Xu, S.Li, R.Shi, H.Liu. *Sig. Transduct. Target. Ther*., **8**, 435 (2023); https://doi.org/10.1038/s41392-023-01654-7
19. S.Fedorenko, A.Stepanov, G.Sibgatullina, D.Samigullin, A.Mukhitov, K.Petrov, R.Mendes, M. Rümmeli, L.Giebeler, B.Weise, T.Gemming, I.Nizameev, K.Kholin, A.Mustafina. *Nanoscale*, **11** (34), 16103 (2019); https://doi.org/10.1039/C9NR05071J
20. J.Kim, H.S.Kim, N.Lee, T.Kim, H.Kim, T.Yu, I.C.Song, W.K.Moon, T.Hyeon. *Angew. Chem., Int Ed*., **47** (44), 8438 (2008); https://doi.org/10.1002/anie.200802469
21. B.Chang, X.Zhang, J.Guo, Y.Sun, H.Tang, Q.Ren, W.Yang. *J. Coll. Interf. Sci*., **377** (1), 64 (2012); https://doi.org/10.1016/j.jcis.2012.03.082
22. A.Stepanov, S.Fedorenko, K.Kholin, I.Nizameev, ADovzhenko, R.Zairov, T.Gerasimova, A.Voloshina, A.Lyubina, G.Sibgatullina, D.Samigullin, A.Mustafina. *Front. Chem. Sci. Eng.*, **17** (12), 2144 (2023); https://doi.org/10.1007/s11705-023-2362-4
23. S Fedorenko, A.Stepanov, O.Bochkova, K.Kholin, A.Dovjenko, R.Zairov, I.Nizameev, T.Gerasimova, I.Strelnik, A.Voloshina, A.Sapunova, S.Gumerova, A.Gubaidullin, S.Fedosimova, V.Evtugyn, A.Toropchina, A.Karasik, A.Mustafina. *Coll. Surf. A: Physicochem. Eng. Aspects*, **626**, 126996 (2021); https://doi.org/10.1016/j.colsurfa.2021.126996
24. S.Fedorenko, D.Farvaeva, A.Stepanov, O.Bochkova, K.Kholin, I.Nizameev, S.Drobyshev, T.Gerasimova, A.Voloshina, E.Fanizza, N.Depalo, G.Sibgatullina, D.Samigullin, K.Petrov, A.Gubaidullin, A.Mustafina. *J. Photochem. Photobiol. A: Chem.*, **433**, 114187 (2022); https://doi.org/10.1016/j.jphotochem.2022.114187
25. H.Tang, C.Li, Y.Zhang, H.Zheng, Y.Cheng, J.Zhu, X.Chen, Z.Zhu, J.-G.Piao, F.Li. *Theranostics*, **10** (21), 9865 (2020); https://doi.org/10.7150/thno.46771
26. O.Bochkova, A.Stepanov, A.Khazieva, B.Akhmadeev, I.Ismaev, K.Kholin, I.Nizameev, A.Sapunova, A.Voloshina, A.Laskin, D.Smekalov, M.Tarasov, Y.Budnikova, A.Mustafina. *Mater. Today Chem.*, **33**, 101706 (2023); https://doi.org/10.1016/j.mtchem.2023.101706
27. R.Mallik, M.Saha, B.Ghosh, N.Chauhan, H.Mohan, S.S.Kumaran, C.Mukherjee. *Small*, **21** (7), 2401787 (2025); https://doi.org/10.1002/smll.202401787
28. O.Bochkova, A.Stepanov, A.Bebyakina, K.Kholin, I.Nizameev, A.Voloshina, A.Parfenov, M.Tarasov, Y.Budnikova, M.Abakumov, V.Evtugyn, A.Gubaidullin, T.Khaybullin, M.Bochkov, E.Karalin, A.Mustafina. *Coll. Surf. A: Physicochem. Eng. Aspects*, **727**, 138232 (2025); https://doi.org/10.1016/j.colsurfa.2025.138232
29. K.Poon, A.Gupta, W.S.Price, H.Zreiqat, G.Singh. *Coord. Chem. Revs*., **500**, 215548 (2024); https://doi.org/10.1016/j.ccr.2023.215548
30. E.Wetterskog, M.Agthe, A.Mayence, J.Grins, D.Wang, S.Rana, A.Ahniyaz, G.Salazar-Alvarez, L.Bergström. *Sci. Technol. Adv. Mater*., **15** (5), 055010 (2014); https://doi.org/10.1088/1468-6996/15/5/055010
31. L.M.Bronstein, X.Huang, J.Retrum, A.Schmucker, M.Pink, B.D.Stein, B.Dragnea. *Chem. Mater.*, **19** (15), 3624 (2007); https://doi.org/10.1021/cm062948j
32. M.Yang, L.Gao, K.Liu, C.Luo, Y.Wang, L.Yu, H.Peng, W.Zhang. *Talanta*, **131**, 661 (2015); https://doi.org/10.1016/j.talanta.2014.08.042
33. F.Chen, W.Bu, Y.Chen, Y.Fan, Q.He, M.Zhu, X.Liu, L.Zhou, S.Zhang, W.Peng, J.Shi. *Chemistry – An Asian J*., **4** (12), 1809 (2009); https://doi.org/10.1002/asia.200900276
34. R.G.Mendes, B.Koch, A.Bachmatiuk, A.A.El-Gendy, Y.Krupskaya, A.Springer, R.Klingeler, O Schmidt, B.Büchner, S.Sanchez, M.H.Rümmeli. *Biochim. Biophys. Acta (BBA) – General Subjects*, **1840** (1), 160 (2014); https://doi.org/10.1016/j.bbagen.2013.08.025
35. H.L.Ding, Y.X.Zhang, S.Wang, J.M.Xu, S.C.Xu, G.H.Li. *Chem. Mater.*, **24** (23), 4572 (2012); https://doi.org/10.1021/cm302828d
36. K.Katagiri, M.Narahara, K.Sako, K.Inumaru. *J. Sol–Gel. Sci. Technol*., **84** (1), 110 (2017); https://doi.org/10.1007/s10971-017-4479-8
37. S.V.Fedorenko, A.S.Stepanov, O.D.Bochkova, A.R.Mustafina. *Colloid J*., **84** (5), 611 (2022); https://doi.org/10.1134/S1061933X22700077
38. W.Stöber, A.Fink, E.Bohn. *J. Coll. Interface Sci*., **26** (1), 62 (1968); https://doi.org/10.1016/0021-9797(68)90272-5
39. F.J.Arriagada, K.Osseo-Asare. *Coll. Surf. A: Physicochem. Eng. Aspects*, **154** (3), 311 (1999); https://doi.org/10.1016/S0927-7757(98)00870-X
40. R.P.Bagwe, C.Yang, L.R.Hilliard, W.Tan. *Langmuir*, **20** (19), 8336 (2004); https://doi.org/10.1021/la049137j
41. Md.M.Islam, Md.A.Rahman, Md.A.Alam, Md.M.Rahman, O.T.Mefford, A.Ul-Hamid, J.Miah, H.Ahmad. *ACS Omega*, **9** (19), 20891 (2024); https://doi.org/10.1021/acsomega.3c10082
42. S.L.C.Pinho, S.Laurent, J.Rocha, A.Roch, M.-H.Delville, S.Mornet, L.D.Carlos, L.Vander Elst, R.N.Muller, C.F.G.C.Geraldes. *J. Phys. Chem. C*, **116** (3), 2285 (2012); https://doi.org/10.1021/jp2086413
43. A.Ahmad, H.Bae, I.Rhee. *AIP Adv*., **8** (5), 055019 (2018); https://doi.org/10.1063/1.5027898
44. M.Veverka, K.Závěta, O.Kaman, P.Veverka, K.Knížek, E.Pollert, M.Burian, P.Kašpar. *J. Phys. D: Appl. Phys.*, **47** (6), 065503 (2014); https://doi.org/10.1088/0022-3727/47/6/065503
45. S.M.Kandil, H.M.Diab, A.M.Mahfoz, A.Elhawatky, E.M.Abdou. *Pharm. Res*., **41** (7), 1475 (2024); https://doi.org/10.1007/s11095-024-03733-y
46. A.Villanueva, P.De La Presa, J.M.Alonso, T.Rueda, A.Martínez, P Crespo, M.P.Morales, M.A.Gonzalez-Fernandez, J.Valdés, G.Rivero. *J. Phys. Chem. C*, **114** (5), 1976 (2010); https://doi.org/10.1021/jp907046f
47. A.Narita, K.Naka, Y.Chujo. *Coll. Surf. A: Physicochem. Eng. Aspects*, **336** (1–3), 46 (2009); https://doi.org/10.1016/j.colsurfa.2008.11.013
48. H.M.Joshi, M.De, F.Richter, J.He, P.V.Prasad, V.P.Dravid. *J. Nanopart. Res*., **15** (3), 1448 (2013); https://doi.org/10.1007/s11051-013-1448-1
49. H.Yang, Y.Zhuang, Y.Sun, A.Dai, X.Shi, D.Wu, F.Li, H.Hu, S.Yang. *Biomaterials*, **32** (20), 4584 (2011); https://doi.org/10.1016/j.biomaterials.2011.03.018
50. H.Jang, C.Lee, G.-E.Nam, B.Quan, H.J.Choi, J.S.Yoo, Y.Piao. *J. Nanopart. Res*., **18** (2), 41 (2016); https://doi.org/10.1007/s11051-016-3353-x
51. T.-H.Shin, J.Choi, S.Yun, I.-S.Kim, H.-T.Song, Y.Kim, K.I.Park, J.Cheon. *ACS Nano*, **8** (4), 3393 (2014); https://doi.org/10.1021/nn405977t
52. J.Choi, J.-H.Lee, T.-H.Shin, H.-T.Song, E.Y.Kim, J.Cheon. *J. Am. Chem. Soc.*, **132** (32), 11015 (2010); https://doi.org/10.1021/ja104503g
53. A.Stepanov, S.Fedorenko, R.Mendes, M.Rümmeli, L.Giebeler, B.Weise, T.Gemming, S.Dutz, D.Zahn, I.Ismaev, R.Amirov, KKholin, A.Voloshina, A.Sapunova, S.Solovieva, A.Mustafina. *J. Chem. Sci*., **133** (2), 43 (2021); https://doi.org/10.1007/s12039-021-01904-7
54. S.Fedorenko, A.Stepanov, R.Zairov, O.Kaman, R.Amirov, I.Nizameev, K.Kholin, I.Ismaev, A.Voloshina, A.Sapunova, M.Kadirov, A.Mustafina. *Coll. Surf. A: Physicochem. Eng. Aspects*, **559**, 60 (2018); https://doi.org/10.1016/j.colsurfa.2018.09.044
55. O.Bochkova, A.Stepanov, A.Bebyakina, D.Smekalov, K.Kholin, I.Nizameev, A.Romashchenko, E.Zavjalov, A.Lubina, A.Voloshina, O.Tyapkina, M.Tarasov, T.Sultanov, M.Rümmeli, V.Salnikov, Y.Budnikova, A.Mustafina. *J. Alloys Compd*., **1008**, 176581 (2024); https://doi.org/10.1016/j.jallcom.2024.176581

56. S.Fedorenko, J.Elistratova, A.Stepanov, A.Khazieva, M.Mikhailov, M.Sokolov, K.Kholin, I.Nizameev, R.Mendes, M.Rümmeli, T.Gemming, B.Weise, L.Giebeler, D.Mikhailova, S.Dutz, D.Zahn, A.Voloshina, A.Sapunova, A.Daminova, S.Fedosimova, A.Mustafina. *Mater. Sci. Eng: C*, **117**, 111305 (2020); https://doi.org/10.1016/j.msec.2020.111305
57. M.Wang, M.Deng. *Mater. Lett*., **309**, 131358 (2022); https://doi.org/10.1016/j.matlet.2021.131358
58. Q.M.Ahkam, E.U.Khan, J.Iqbal, A.Murtaza, M.T.Khan. *Phys. B: Condensed Matter*., **572**, 161 (2019); https://doi.org/10.1016/j.physb.2019.07.044
59. F.Ye, S.Laurent, A.Fornara, L.Astolfi, J.Qin, A.Roch, A.Martini, M.S.Toprak, R.N.Muller, M.Muhammed. *Contrast Media Mol. Imaging*, **7** (5), 460 (2012); https://doi.org/10.1002/cmmi.1473
60. K.Laxmanan, R.Vivek, N.P.Sarathy, H.W.Kang. *Mater. Today Commun*., **47**, 113244 (2025); https://doi.org/10.1016/j.mtcomm.2025.113244
61. G.Li, X.Li, Z.Lou, J.Xu, Y.Ma, X.Li, Q.Liu, T.Sun. *Mater. Today Bio*., **34**, 102197 (2025); https://doi.org/10.1016/j.mtbio.2025.102197
62. K.Liu, K.Liu, J.Liu, Q.Ren, Z.Zhao, X.Wu, D.Li, F.Yuan, K.Ye, B.Li. *Nanoscale*, **12** (5), 2902 (2020); https://doi.org/10.1039/C9NR08737K
63. M.Yu, Z.Zhao. *J. Lumin.*, **225**, 117361 (2020); https://doi.org/10.1016/j.jlumin.2020.117361
64. S.Wang, J.Liu, S.Qiu, J.Yu. *J. Photochem. Photobiol. B: Biology*, **199**, 111583 (2019); https://doi.org/10.1016/j.jphotobiol.2019.111583
65. E.Fanizza, R.Mastrogiacomo, O.Pugliese, A.Guglielmelli, L.De Sio, R.Castaldo, M.Scavo, M.Giancaspro, F.Rizzi, G.Gentile, F.Vischio, L.Carrieri, I.De Pasquale, G.Mandriota, F.Petronella, C.Ingrosso, M.Lavorgna, R.Comparelli, M.Striccoli, M.Curri, N.Depalo. *Nanomaterials*, **12** (15), 2545 (2022); https://doi.org/10.3390/nano12152545
66. O.Dimitriev, Y.Slominskii, M.Giancaspro, F.Rizzi, N.Depalo, E.Fanizza, T.Yoshida. *Nanomaterials*, **13** (3), 510 (2023); https://doi.org/10.3390/nano13030510
67. F.Rizzi, E.Fanizza, M.Giancaspro, N.Depalo, M.L.Curri, B.González, M.Colilla, I.Izquierdo-Barba, M.Vallet-Regí. *Micropor. Mesopor. Mater*., **383**, 113414 (2025); https://doi.org/10.1016/j.micromeso.2024.113414
68. Y.Zhang, Z.Hou, Y.Ge, K.Deng, B.Liu, X.Li, Q.Li, Z.Cheng, P.Ma, C.Li, J.Lin. *ACS Appl. Mater. Interfaces*, **7** (37), 20696 (2015); https://doi.org/10.1021/acsami.5b05522
69. I.M.El-Nahhal, J.K.Salem, S.Kuhn, T.Hammad, R.Hempelmann, S.Al Bhaisi. *J. Sol–Gel Sci. Technol*., **79** (3), 573 (2016); https://doi.org/10.1007/s10971-016-4034-z
70. B.T.Fashina, A.P.Baldo, H.Watts, K.Leung, J.D.Kubicki, A.G.Ilgen. *Micropor. Mesopor. Mater*., **387**, 113538 (2025); https://doi.org/10.1016/j.micromeso.2025.113538
71. R.Guillet-Nicolas, M.Laprise-Pelletier, M.M.Nair, P.Chevallier, J.Lagueux, Y.Gossuin, S.Laurent, F.Kleitz, M.-A.Fortin. *Nanoscale*, **5** (23), 11499 (2013); https://doi.org/10.1039/c3nr02969g
72. J.Chandra, S.M.Teoh, P.Kuo, L.Tolley, A.A.Bashaw, Z.K.Tuong, Y.Liu, Z.Chen, J.W.Wells, C.Yu, I.H.Frazer, M.Yu. *J. Immunol*., **206** (5), 987 (2021); https://doi.org/10.4049/jimmunol.2000355
73. J.Andas, F.Adam, I.Ab.Rahman. *Appl. Surf. Sci*., **315**, 154 (2014); https://doi.org/10.1016/j.apsusc.2014.07.118
74. L.Yao, G.Xu, W.Dou, Y.Bai. *Coll. Surf. A: Physicochem. Eng. Aspects*, **316** (1–3), 8 (2008); https://doi.org/10.1016/j.colsurfa.2007.08.016
75. F.J.Arriagada, K.Osseo-Asare. *J. Coll. Interface Sci*., **211** (2), 210 (1999); https://doi.org/10.1006/jcis.1998.5985
76. K.L.Chee, N.A.Mohd Zabidi, M.S.Chandra. *DDF*, **312–315**, 370 (2011); https://doi.org/10.4028/www.scientific.net/DDF.312-315.370
77. N.Ghavidel Hajiagha, A.Mahmoudi, M.R.Sazegar, M.M.Pouramini. *Micropor. Mesopor. Mater*., **274**, 43 (2019); https://doi.org/10.1016/j.micromeso.2018.07.018
78. O.Bochkova, M.Khrizanforov, A.Gubaidullin, T.Gerasimova, I.Nizameev, K.Kholin, A.Laskin, Y.Budnikova, O.Sinyashin, A.Mustafina. *Nanomaterials*, **10** (7), 1338 (2020); https://doi.org/10.3390/nano10071338
79. P.Caravan, C.T.Farrar, L.Frullano, R.Uppal. *Contrast Media Mol. Imaging*, **4** (2), 89 (2009); https://doi.org/10.1002/cmmi.267
80. P.Caravan. *Invest. Radiol*., **59** (2), 187 (2024); https://doi.org/10.1097/RLI.0000000000001053
81. M.Botta, F.Carniato, D.Esteban-Gómez, C.Platas-Iglesias, L.Tei. *Future Med. Chem*., **11** (12), 1461 (2019); https://doi.org/10.4155/fmc-2018-0608
82. M.N.Khrizanforov, S.V.Fedorenko, A.R.Mustafina, V.V.Khrizanforova, K.V.Kholin, I.R.Nizameev, T.V.Gryaznova, V.V.Grinenko, Y.H.Budnikova. *RSC Adv.*, **9** (39), 22627 (2019); https://doi.org/10.1039/C9RA03421H
83. X.W.Li, W.R.Zhao, Y.J.Liu, X.H.Liu, P.Shi, Y.S.Li, J.L.Shi. *J. Mater. Chem. B*, **4** (24), 4313 (2016); https://doi.org/10.1039/C6TB00718J
84. D.Zhang, W.Zhang, X.Wu, Q.Li, Z.Mu, F.Sun, M.Zhang, G.Liu, L.Hu. *Int. J. Nanomed.*, **16**, 3457 (2021); https://doi.org/10.2147/IJN.S306269
85. R.R.Zairov, B.S.Akhmadeev, S.V.Fedorenko, A.R Mustafina. *Chem. Eng. J*., **459**, 141640 (2023); https://doi.org/10.1016/j.cej.2023.141640
86. R.Antony, S.T.D.Manickam, S.Balakumar. *J. Inorg. Organomet. Polym*., **27** (2), 418 (2017); https://doi.org/10.1007/s10904-016-0482-8
87. C.Freire, C.Pereira, S.Rebelo. *Catalysis*, **24**, 116 (2012); https://doi.org/10.1039/9781849734776-00116
88. R.J.Lewis, G.J.Hutchings. *ChemCatChem*, **11** (1), 298 (2019); https://doi.org/10.1002/cctc.201801435
89. R.J.Lewis, K.Ueura, Y.Fukuta, S.J.Freakley, L.Kang, R.Wang, Q.He, J.K.Edwards, D.J.Morgan, Y.Yamamoto, G.J.Hutchings. *ChemCatChem*, **11** (6), 1673 (2019); https://doi.org/10.1002/cctc.201900100
90. R.Mallik, M.Saha, C.Mukherjee. *ACS Appl. Bio Mater.*, **4** (12), 8356 (2021); https://doi.org/10.1021/acsabm.1c00937
91. R.Mallik, M.Saha, V.Singh, H.Mohan, S.S.Kumaran, C.Mukherjee. *J. Mater. Chem. B*, **11** (34), 8251 (2023); https://doi.org/10.1039/D3TB01289A
92. L.Chong, Y.-W.Jiang, D.Wang, P.Chang, K.Xu, J.Li. *J. Nanobiotechnol*., **21** (1), 401 (2023); https://doi.org/10.1186/s12951-023-02122-8
93. F.Liu, Q.Xiang, Y.Luo, Y.Luo, W.Luo, Q.Xie, J.Fan, H.Ran, Z.Wang, Y.Sun. *J. Nanobiotechnol*., **21** (1), 165 (2023); https://doi.org/10.1186/s12951-023-01932-0
94. N.Zhu, H.Cai, P.He, Y.Fang. *Anal. Chim. Acta*, **481** (2), 181 (2003); https://doi.org/10.1016/S0003-2670(03)00123-5
95. Y.Budnikova, O.Bochkova, M.Khrizanforov, I.Nizameev, K.Kholin, T.Gryaznova, A.Laskin, Y.Dudkina, S.Strekalova, S.Fedorenko, A.Kononov, A.Mustafina. *ChemCatChem*, **11** (22), 5615 (2019); https://doi.org/10.1002/cctc.201901391
96. M.Mureseanu, M.Filip, I.Bleotu, C.I.Spinu, A.H.Marin, I.Matei, V.Parvulescu. *Nanomaterials*, **13** (12), 1884 (2023); https://doi.org/10.3390/nano13121884
97. D.Lalli, G.Ferrauto, E.Terreno, F.Carniato, M.Botta. *J. Mater. Chem. B*, **9** (43), 8994 (2021); https://doi.org/10.1039/D1TB01600H
98. J.Lu, C.Ni, J.Huang, Y.Liu, Y.Tao, P.Hu, Y.Wang, S.Zheng, M.Shi. *Front. Bioeng. Biotechnol.*, **9**, 752982 (2021); https://doi.org/10.3389/fbioe.2021.752982
99. D.Tang, L.Zhang, Y.Zhang, Z.-A.Qiao, Y.Liu, Q.Huo. *J. Coll. Interface Sci*., **369** (1), 338 (2012); https://doi.org/10.1016/j.jcis.2011.12.014
100. D.Tang, W.Zhang, Z.Qiao, Y.Liu, Q.Huo. *RSC Adv.*, **6** (20), 16461 (2016); https://doi.org/10.1039/C5RA25135D

101. G.Vala, R.N.Jadeja, A.A.Puranik, R.J. Butcher. *J. Mol. Struct*., **1322**, 140513 (2025); https://doi.org/10.1016/j.molstruc.2024.140513
102. J.F.Díaz, K.J.Balkus, F.Bedioui, V.Kurshev, L.Kevan. *Chem. Mater.*, **9** (1), 61 (1997); https://doi.org/10.1021/cm960228e
103. S.Santra, P.Zhang, K.Wang, R.Tapec, W.Tan. *Anal. Chem.*, **73** (20), 4988 (2001); https://doi.org/10.1021/ac010406+
104. M.-Y.Chen, Z.-Z.Chen, W.Wang, L.Zhu, H.-W.Tang, D.-W.Pang. *Chin. J. Anal. Chem*., **42** (3), 326 (2014); https://doi.org/10.1016/S1872-2040(13)60715-X
105. S.Fedorenko, A.Stepanov, O.Bochkova, K.Kholin, I.Nizameev, A.Voloshina, O.Tyapkina, D.Samigullin, S.Kleshnina, B.Akhmadeev, A.Romashchenko, E.Zavjalov, R.Amirov, A.Mustafina. *Nanomedicine: Nanotechnol. Biology Medicine*, **49**, 102665 (2023); https://doi.org/10.1016/j.nano.2023.102665
106. A.R.Mustafina, S.V.Fedorenko, O.D.Konovalova, A.Yu.Menshikova, N.N.Shevchenko, S.E.Soloveva, A.I.Konovalov, I.S.Antipin. *Langmuir*, **25** (5), 3146 (2009); https://doi.org/10.1021/la8032572
107. S.V.Fedorenko, S.L.Grechkina, A.R.Mustafina, K.V.Kholin, A.S.Stepanov, I.R.Nizameev, I.E.Ismaev, M.K.Kadirov, R.R.Zairov, A.N.Fattakhova, R.R.Amirov, S.E.Soloveva. *Coll. Surf. B: Biointerfaces*, **149**, 243 (2017); https://doi.org/10.1016/j.colsurfb.2016.10.025
108. R.Amirov, Z.McMillan, A.Mustafina, I.Chukurova, S.Solovieva, I.Antipin, A.Konovalov. *Inorg. Chem. Commun*., **8** (9), 821 (2005); https://doi.org/10.1016/j.inoche.2005.06.010
109. N.Iki, T.Fujimoto, S.Miyano. *Chem. Lett*., **27** (7), 625 (1998); https://doi.org/10.1246/cl.1998.625
110. O.Bochkova, S.Fedorenko, A.Mikhailov, G.Kostin, M.Mikhailov, M.Sokolov, J.Elistratova, K.Kholin, M.Tarasov, Y.Budnikova, G.Sibgatullina, D.Samigullin, I.Nizameev, V.Salnikov, I.Yakovlev, D.Rozhentsova, A.Lyubina, S.Amerhanova, A.Voloshina, T.Gerasimova, A.Mustafina. *J. Photochem. Photobiol. A: Chem*., **446**, 115147 (2024); https://doi.org/10.1016/j.jphotochem.2023.115147
111. A.R.Mukhametshina, A.R.Mustafina, N.A.Davydov, S.V.Fedorenko, I.R.Nizameev, M.K.Kadirov, V.V.Gorbatchuk, A.I.Konovalov. *Langmuir*, **31** (1), 611 (2015); https://doi.org/10.1021/la503074p
112. O.Bochkova, A.Bebyakina, A.Stepanov, T.Khaybullin, D.Smekalov, B.Faizullin, A.Voloshina, A.Lubina, K.Kholin, I.Nizameev, A.Khamatgalimov, M.Bochkov, E.Karalin, A.Mustafina. *Coll. Surf. B: Biointerfaces*, **264**, 115628 (2026); https://doi.org/10.1016/j.colsurfb.2026.115628